Monatshefte für Chemie 132, 295–304 (2001)

Monatshefte für Chemie
Chemical Monthly

N-Aryl-N-Hydroxy Urethanes as Peroxidase Substrates

Juozas Kulys[1,*], **Heinz-Josef Deussen**[2], **Kastis Krikstopaitis**[1], **Palle Schneider**[2], and **Arturas Ziemys**[3]

[1] Institute of Biochemistry, LT-2600 Vilnius, Lithuania
[2] Novo Nordisk A/S, DK-2880 Bagsværd, Denmark
[3] Vytautas Magnus University, Environmental Faculty, Department of Biology, LT-3500 Kaunas, Lithuania

Summary. N-Aryl-N-hydroxy urethanes (*AHU*s), which are promising N–OH mediators for oxidoreductase catalysis, are electrochemically active redox compounds with a redox potential of 0.35–0.40 V *vs*. SCE (0.59–0.64 V *vs*. NHE). Alkyl substituents in the carbamic acid residue have, as expected, only little influence on the redox potential. The highest potential was noticed for N-hydroxy-N-(4-cyanophenyl)-carbamic acid methyl ester. Recombinant *Coprinus cinereus* peroxidase (rCiP) catalyzes oxidation of the *AHU*s with apparent bimolecular constants k_{ox} of $2.5 \cdot 10^4$–$7.5 \cdot 10^4\, M^{-1}s^{-1}$ at $pH = 8.5$ and 25°C.

Structure-function connectivities of the substrates were analysed within the framework of the *Marcus* cross relationship and by using *ab initio* quantum chemical calculations. An excellent correlation of the redox potentials and the HOMO energies could be found. However, no correlation of $\log(k_{ox})$ with redox potential and HOMO energy was indicated as predicted by theory. This was explained by specific docking of the substrates in the active center of rCiP.

Keywords. Redox potential; Fungal peroxidase; Reactivity; *ab initio* Calculations; Substrate docking.

Introduction

A large variety of different organic redox compounds have been suggested as mediators for peroxidase and laccase catalyzed oxidations [1]. In these reactions, the enzyme catalyzes the oxidation of an organic molecule, the so-called mediator (*M*H). The oxidized mediator then chemically oxidizes the target molecule (non-substrate) and is in turn reduced, thus switching the mediator between its oxidized and reduced states according to Eqs. (1)–(3). In these equations, E_{red} and E_{ox} represent the oxidoreductase in its reduced and oxidized state, *M*H the enzyme substrate, and $M^{\cdot}$ its oxidized state.

$$E_{red} + \text{oxidizer} \rightarrow E_{ox} \tag{1}$$

$$E_{ox} + M\text{H} \rightarrow E_{red} + M^{\cdot} + \text{H}^+ \tag{2}$$

$$M^{\cdot} + \text{target molecule} + \text{H}^+ \rightarrow \text{product} + M\text{H} \tag{3}$$

* Corresponding author

Phenols and aromatic amines are typical substrates for peroxidases and laccases [2, 3]. These enzymes catalyze the oxidation of single electron donors, *e.g.* phenylenediamines, phenothiazines, and phenoxazines [4, 5]. Heterocyclic phenols, *e.g.* aromatic compounds containing an N–OH group, have been suggested earlier as mediators in peroxidase and laccase catalyzed dye and lignin bleaching as well as lignin degradation [1]. The kinetics of the enzymatic oxidation of N-hydroxybenzotriazole (*HBT*) has been investigated [6], and the unexpectedly low reactivity of *HBT* found has been attributed to the large redox potential of this substrate. Derivatives of N-aryl hydroxamic acids, *i.e.* compounds containing an *R*–CO–N(OH)–Ar group, represent another type of N–OH mediators, investigated only very recently [7]. The aim of this work is to explore redox and mediator properties of a new type of redox compounds, the N-aryl-N-hydroxy urethanes (*AHU*s) **1–5** [8]. The kinetics of the oxidation of **1–5** was investigated using a recombinant *Coprinus cinereus* peroxidase (rCiP) with an emphasis on establishing structure-activity relations by using *ab initio* quantum chemical computations and substrate docking calculations.

Results and Discussion

The structures of the investigated *AHU*s **1–5** are depicted in Fig. 1. The redox activity of compounds **1–5** was explored by cyclic voltammetry (CV). The CV curves of **1–4** showed oxidation-reduction peaks which were almost symmetrical, thus revealing the reversible character of the electrochemical conversion and the rather high stability of the oxidized species (shown for **1** in Fig. 2). The calculated redox potentials of **1–4** varied in the range between 0.33 and 0.35 V *vs.* SCE (Table 1).

In contrast to **1–4**, the cathodic peak of **5** was such smaller than the anodic peak at potential scan rates of 50 and 100 mV/s (Fig. 3). A possible explanation for this behaviour could be the low stability of the oxidized species of **5**. Therefore, the formal redox potential of **5** was calculated at a higher scan rate.

The absorption spectra of **1–4**, which all contain an unsubstituted phenyl ring, showed an absorbance at 240–250 nm in their UV/Vis spectra; the absorbance of their oxidized products was found at 282 and 307 nm (Fig. 4). The differences of the extinction coefficients ($\Delta\varepsilon$) of oxidized and reduced compounds at 307 nm are listed in Table 2.

The absorbance of the products showed significant similarity with that of nitrosobenzene (*NB*, Fig. 4). The formation of *NB* can be explained by single-

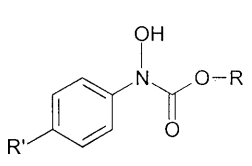

1: *R* = methyl, *R*' = H
2: *R* = ethyl, *R*' = H
3: *R* = 2-propyl, *R*' = H
4: *R* = phenyl, *R*' = H
5: *R* = methyl, *R*' = CN

Fig. 1. Structures of N-aryl-N-hydroxy urethanes **1–5**

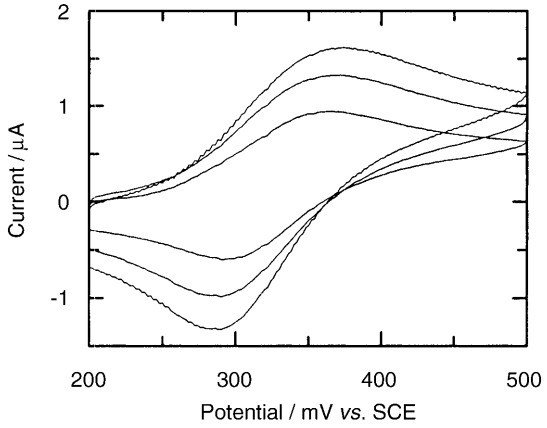

Fig. 2. Cyclic voltammograms of **1** at potential scan rates of 50, 100, and 200 $mV \cdot s^{-1}$ at $pH = 8.5$

Table 1. Cyclic voltammetry of **1–5** in 0.05 *M* borate buffer solution ($pH = 8.5$)

	Scan rate/$mV \cdot s^{-1}$	$E_{p(a)}$/mV	$E_{p(c)}$/mV	$E_{1/2}$/mV
1	50	370	312	341
1	100	378	312	345
1	200	372	306	339
2	50	366	304	335
2	100	370	304	337
2	200	372	298	335
3	50	350	290	320
3	100	366	290	328
3	200	374	284	329
4	50	370	322	346
4	100	378	322	350
4	200	380	322	351
5	50	414	–	–
5	100	422	368	395
5	200	428	370	399

electron oxidation of the respective substrate by the oxidized enzyme (Eq. (4)) followed by disproportionation of the formed radical (Eq. (5)) and reaction of the intermediate with water (Eq. (6)).

$$Ph{-}N(OH){-}C(O)OMe \rightarrow Ph{-}N(O^{\cdot}){-}C(O)OMe + e^{-} + H^{+} \quad (4)$$

$$2\,Ph{-}N(O^{\cdot}){-}C(O)OMe \rightarrow Ph{-}N(OH){-}C(O)OMe + Ph{-}N^{+}(O){-}C(O)OMe \quad (5)$$

$$Ph{-}N^{+}(O){-}C(O)OMe + H_2O \rightarrow Ph{-}NO + HOC(O)OMe + H^{+} + e^{-} \quad (6)$$

Compound **5** showed absorption maxima at 269 and 322 nm. The oxidation of this substrate generated a product with a decreased absorbance at 269 nm and an increased absorbance at 307 nm (Fig. 5).

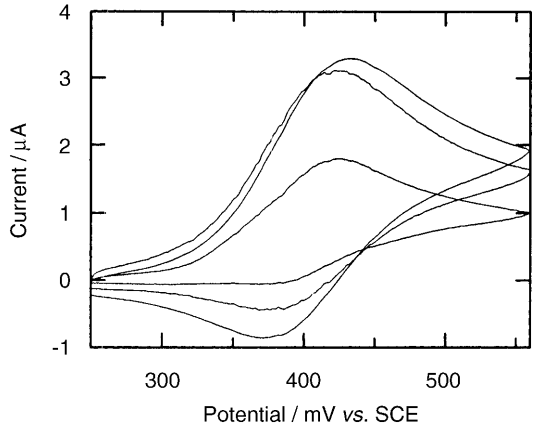

Fig. 3. Cyclic voltammograms of **5** at potential scan rates of 50, 100, and 200 $mV \cdot s^{-1}$ at $pH = 8.5$

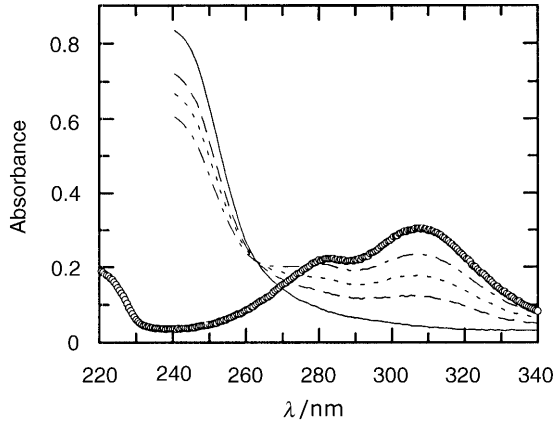

Fig. 4. Absorbance of **2** at $pH = 8.5$; the first spectrum corresponds to 0.1 m*M* of **2**, the others to the mixture obtained by addition of 40 n*M* rCiP and 0.1 m*M* hydrogen peroxide (recorded at $t = 10$, 20, and 35 min); o: 50 μ*M* nitrosobenzene

Table 2. Electrochemical and kinetic parameters of **1–5** at $pH = 8.5$ and 25°C

	$E_{1/2}$ / mV *vs.* SCE	λ_{max} / nm	$\Delta\varepsilon$ / $mM^{-1} \cdot cm^{-1}$	[rCiP] / n*M*	k_{ox} / $M^{-1} \cdot s^{-1}$
1	345	307	4.9	250	$2.3 \pm 0.2 \cdot 10^4$
2	337	307	4.8	250	$7.5 \pm 0.5 \cdot 10^4$
3	328	307	4.3	250	$3.2 \pm 0.2 \cdot 10^4$
4	351	307	3.6	250	$4.2 \pm 0.2 \cdot 10^4$
5	396	307	9.0	125	$2.5 \pm 0.5 \cdot 10^4$

The kinetics of the rCiP-catalyzed oxidation of **1–5** was monitored by the absorbance increase at 307 nm. The initial rate increased linearly up to 200 μ*M* of **1** and **3** (Fig. 6). Apparent oxidation constants (k_{ox}) were calculated as slope/[*E*] and are listed in Table 2. The initial oxidation rate of **2**, **4**, and **5** showed saturation

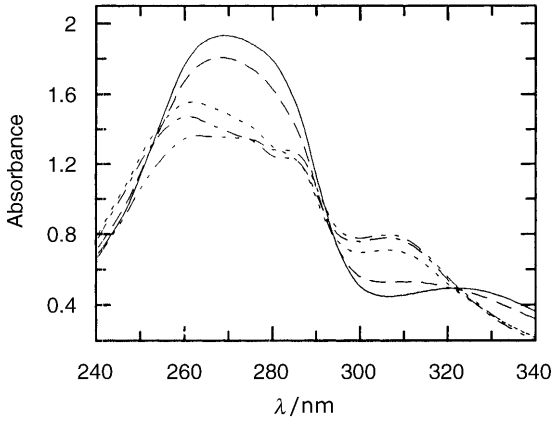

Fig. 5. Absorbance spectrum of **5** at $pH = 8.5$ after addition of 0.1 m*M* 5, 40 n*M* rCiP, and 0.1 m*M* hydrogen peroxide; time between measurements: 10–20 min

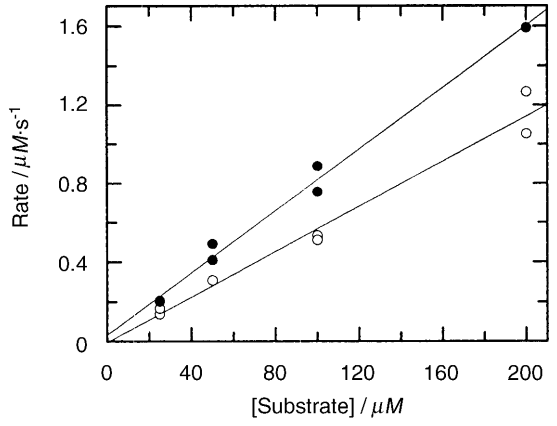

Fig. 6. Dependence of oxidation rate on substrate concentration of **1** (o) and **3** (●) at $pH = 8.5$; rCiP: 250 n*M*, hydrogen peroxide: 0.1 m*M*

behaviour (Fig. 7). Kinetic parameters for these substrates were calculated according to the *Michaelis-Menten* equation. The apparent K_m values were 336 μ*M* for **2**, 409 μ*M* for **4**, and 415 μ*M* for **5**.

The electrochemical investigations of **1–5** demonstrated that all compounds are redox active. The alkyl substituents in the carbamic acid residue had only little influence on the redox potential (Table 2). The highest redox potential could be observed for **5** which contains an electron-withdrawing cyano group in *p*-position. The rate constants of the rCiP-catalyzed oxidation of **1–5** changed in the range of $2.3 \cdot 10^4$ to $7.5 \cdot 10^4\, M^{-1}s^{-1}$ (Table 2). The *Marcus* theory of electron transfer predicts a correlation of $\log(k_{ox})$ with the free energy of reaction [9]. However, no satisfactory correlation could be found between $\log(k_{ox})$ and the redox potential for all substrates.

In an attempt to explain the electrochemical behavior and enzymatic reactivity of **1–5**, *ab initio* calculations with respect to **1** and **4** were performed. The calculations showed that the geometries of the reduced states of **1** and **4** are almost

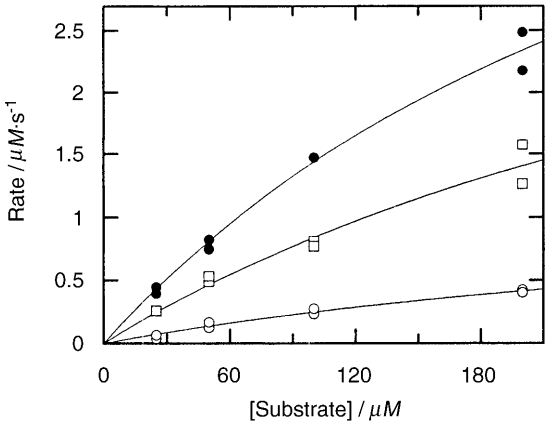

Fig. 7. Dependence of oxidation rate on the concentration of **2** (●), **4** (□), and **5** (o) at $pH = 8.5$; rCiP: 250 (**2**, **4**) and 125 n*M* (**5**), hydrogen peroxide: 0.1 m*M*

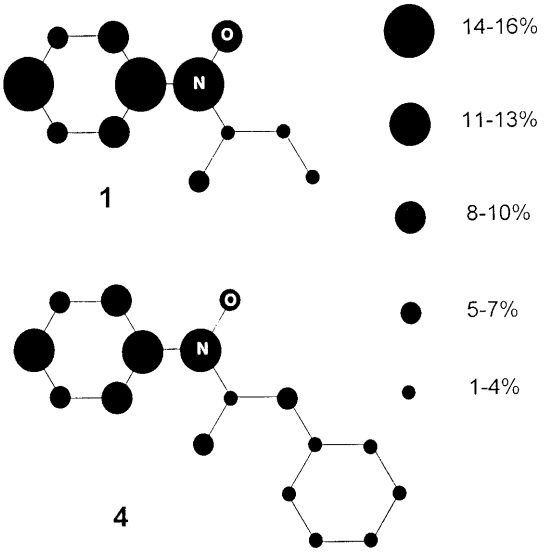

Fig. 8. Contribution of the atomic orbitals to the HOMOs of **1** and **4**

planar; in the radical state, the structures became completely planar. The calculated energies of the HOMOs were in the range of −0.3054 au and −0.3305 au.The LUMOs changed in the range between of 0.0897 au and 0.1424 au. In accordance with the molecular orbital coefficients, the HOMO structures of **1** and **4** are mainly derived from the N-aryl fragments (Fig. 8). The largest contributions result from N, C6, and C9. The calculations showed a strong conjugation of the π-electrons of the N-aryl and N–OH group; the carbonyl group contributed very little. The results presented in Fig. 8 show that the phenyl substituent in ester groups, as *e.g.* in **4**, does not make an essential contribution to the HOMO. The calculations also showed that during the oxidation the main rearrangements in geometry and electronic structure take place in the nearest vicinity of the N–OH fragment. As a consequence, the

N–O bond length becomes shorter by about 0.06–0.08 Å and it is more similar to a double bond.

The electrochemical oxidation of *AHU*s was associated with electron transfer from the HOMO. Therefore, the values of redox potential were correlated with the HOMO energy. The high value of the correlation coefficient ($R^2 = 0.9900$) demonstrated good coincidence between experimentally determined and calculated parameters. In contrast, no significant correlation was found between $\log(k_{ox})$ and the HOMO energy. This fact, in combination with the bad correlation of $\log(k_{ox})$ with the redox potential, permits to hypothesize that the enzymatic reactivity is determined by specific docking of the substrates in the active center of rCiP.

The docking of benzhydroxamic acid (*BHA*) in the active center of *Arthromyces ramosus* peroxidase (ARP) has been investigated recently [10]. A crystal structure of ARP and rCiP has been found to be similar [10, 11]. Therefore, a possible docking of *AHU*s in the active center of rCiP was analyzed analogously to the docking in the active center of ARP. To test whether a program can correctly predict the experimentally determined binding mode, we first investigated the binding mode for *BHA*. The calculated docking completely fitted the ARP and *BHA* structure if the X-ray structure of ARP in the complex with benzhydroxamic acid was used [10].

The docking of **4** to both 1ARP (ARP structure) and 1HSR (structure in the complex ARP and benzhydroxamic acid) produced three clusters near Pro91 and Ile153 (Fig. 9). The mean docking energy of these clusters was −30.2, −28.9, and −27.1 $kJ \cdot mol^{-1}$ (Table 3). An additional cluster was found to be located at the entrance to the heme pocket; its mean docking energy was $-27.90\,kJ \cdot mol^{-1}$. Docking of **4** to the 1HSR structure resulted in the formation of analogous clusters; however, the docking energy was larger. In both structures the clusters are located at the distal side of heme at the entrance to the active center. The N-aryl fragment in the **4**/1ARP complex was spaced by about 9.2 Å from the water molecule, the O-aryl fragment being closer to the heme than the N-aryl fragment. The distance of the *meta*-carbon atom in the O-aryl fragment was 3.73 Å from the heme and 4.72 Å

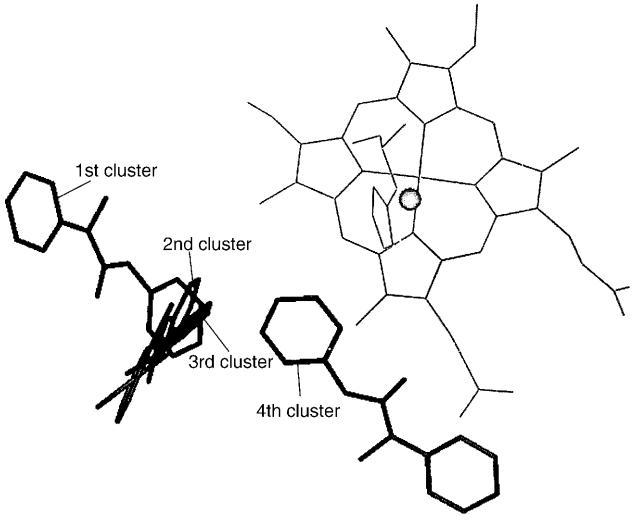

Fig. 9. Docking of **4** in the ARP structure

Table 3. Docking energy of N-aryl-N-hydroxy urethanes in the active center of ARP

	$\frac{E_{1ARP}}{kJ \cdot mol^{-1}}$	Location	$\frac{E_{1HSR}}{kJ \cdot mol^{-1}}$	Location
4	−30.25	Pro91, Ile153	−29.54	Pro91, Ile153
4	−28.95	Pro91, Ile153	−28.99	Pro91, Ile153
4	−27.07	Pro91, Ile153	−27.70	Pro91, Ile153
4	−27.90	Entrance	−26.90	Entrance
1	−21.87 to −26.77	Pro91, Ile153	−21.83 to −25.39	Pro91, Ile153
1	−22.25	Asp98, Thr99, Lys49	−22.08	Asp98, Thr99, Lys49

from the water molecule in the **4**/1HSR complex. For 1ARP, the respective distances were 3.73 and 3.71 Å.

The calculations of the docking of **1** in 1ARP and 1HSR structures revealed that about 95% of the substrate combines in a small pocket at Pro91 and Ile153. The mean docking energy of these clusters changes from -21.87 to $-26.77\,kJ \cdot mol^{-1}$ or from -21.83 to $-25.39\,kJ \cdot mol^{-1}$ (Table 3). A small amount of the substrate can also combine at the residues of Asp98, Thr99, and Lys49. In this complex, the N-aryl fragment is located at a distance of 14 Å from the heme and the water molecule.

The docking results show that N-aryl fragments of **1** and **4** are located far away from the heme. Since the HOMO of the *AHU*s is located mostly on this fragment, the low reactivity of the substrates may be explained by the large electron transfer distance. Since the redox potential of the substrates changes little, their docking in the active center determines the electron transfer rate.

Experimental

N-Hydroxy-N-phenyl carbamic acid methyl ester (**1**) [12], N-hydroxy-N-phenyl carbamic acid ethyl ester (**2**) [13, 14], N-hydroxy-N-phenyl carbamic acid 2-propyl ester (**3**) [15, 16], and N-hydroxy-N-phenyl carbamic acid phenyl ester (**4**) [17] were all synthesized according to literature procedures. They were identified by ^1H NMR and ^{13}C NMR spectroscopy (Varian Mercury 400) and by their melting points. Elemental analyses (C, H, N) were determined by PD Analytical Laboratories (Novo Nordisk A/S, Måløv); they agreed satisfactorily with the calculated values. Melting points were determined on a Büchi 510 apparatus and are uncorrected. All chemicals used were obtained from commercial sources (Aldrich, Fluka, Avocado). Thin-layer chromatography was performed using Alugram SIL G/UV_{254} TLC plates from Macherey-Nagel.

N-Hydroxy-N-(4-cyanophenyl)-carbamic acid methyl ester (**5**; $C_9H_8N_2O_3$)

A solution of 3.13 g N-4-(cyanophenyl)-hydroxylamine (21.1 mmol) in 30 cm^3 *THF* was synthesized following the procedure described for the preparation of N-4-phenylhydroxylamine [7, 18]. A slurry of 4.6 g $NaHCO_3$ in 7 cm^3 H_2O was added to the solution. The mixture was cooled to −0°C, and 1.43 cm^3 methyl chloroformate (21.1 mmol) were added dropwise. Stirring was continued overnight; then, 30 cm^3 of 8% NaOH were added over a period of 45 min. The aqueous phase was separated, petroleum ether (60 cm^3) was added to the *THF*-phase, and the aqueous phase was separated again. The organic phase was extracted twice with 40 cm^3 8% NaOH. The combined aqueous phases were washed with CH_2Cl_2 and neutralized with HCl under cooling. The acidified H_2O-phase was extracted 3 times with 60 cm^3 CH_2Cl_2. The combined organic phases were dried over $MgSO_4$, filtered, and the solvent was removed in vacuum to give crude **5**. The compound was crystallized from toluene/heptane to afford 2.69 g of white crystals (66%).

Mp.: 118–121°C; ^{1}H NMR (400 MHz, δ, $CDCl_3$): 7.71 (d, 2H), 7.63 (d, 2H), 3.93 (s, 3H) ppm; ^{13}C NMR (100 MHz, δ, $CDCl_3$): 154.16, 143.89, 132.52, 119.01, 118.54, 107.17, 54.22 ppm.

Recombinant fungal peroxidase from *Coprinus cinereus* (rCiP) was a highly purified product of Novo Nordisk A/S, Denmark; its *Reinheit-Zahl* (A_{405}/A_{280}) was 2.61. The concentration of rCiP was determined spectrophotometrically at 405 nm assuming a molar absorbance of $1.08 \cdot 10^5\, M^{-1} \cdot cm^{-1}$ [19]. Solutions of H_2O_2 were prepared from perhydrol (30%), and concentrations were established using a molar absorbance of $39.4\, M^{-1} \cdot cm^{-1}$ at 240 nm [20].

The steady-state kinetic measurements of the oxidations were performed by a spectrophotometric method. Kinetic curves and absorption spectra were registered using a computer-assisted spectrophotometer (Gilford Instrument model 2600, Gilford Instrument Lab., USA). The substrates were dissolved in methanol with the exception of **1** which was dissolved in buffer solution. The amount of methanol in the final solution was 0.5% (v/v). The reaction was initiated by addition of H_2O_2. The measurements were carried out at 25±0.1°C in 0.05 *M* borate buffer ($pH = 8.5$). The kinetic data (absorbance change) were approximated by a third order polynomial function; the relative error of approximation did not exceed 0.2%. The calculated initial steady-state rate was used for further analysis. If the initial rate was a linear function of the substrate concentration, an apparent bimolecular rate constant (k_{ox}) was calculated from its slope. If the rate showed a saturating character, an apparent *Michaelis* constant (K_m) and a catalytic constant (k_{cat}) was calculated according to the *Michaelis-Menten* equation. In this case an apparent bimolecular rate constant (k_{ox}) was defined as the ratio of k_{cat}/K_m. All data are presented as mean values ± standard deviation.

The cyclic voltammograms were recorded in a three-electrode circuit using a computer-controlled electroanalytical system (Cypress Systems Inc., USA) and a glassy carbon electrode (model Cs-1087, Cypress Systems Inc., USA). A saturated calomel electrode (SCE, saturated with KCl, mod. K-401, Radiometer, Denmark) was used as a reference. As an auxiliary electrode, a Pt-wire (diameter 0.2 mm, length 4 cm) mounted on the end of the reference electrode was used. The electrode potential was varied from 200 to 800 mV, the potential scan rate was 100 mV/s. The formal redox potential ($E_{1/2}$) was estimated by using the relationship $E_{1/2} = (E_{p(a)} + E_{p(c)})/2$, where $E_{p(a)}$ and $E_{p(c)}$ are the anodic and cathodic peak potentials, respectively.

Ab initio calculations of electronic structures and the energies of **1–5** were performed using the Gaussian 94 W package [21]. The optimization of geometry was accomplished using HF (*Hartree-Fock*) theory and the 3-21 G basis set. The optimized geometry of molecules was used for the further *ab initio* HF calculations with the 6-31 G basis set. The geometry of the radicals was optimized under the ROHF theory and 3-21 G, the energetic parameters were calculated employing the ROHF/6-31 G model.

The simulations of substrate docking in the active center of *Arthromyces ramosus* peroxidase (ARP) were performed with AutoDock 3.0 [22–24]. The crystal data of ARP (1ARP) and the ARP/benzhydroxamic acid (1HSR) complex [25, 26] were downloaded from the Protein Data Bank. All water molecules in the active center of ARP were removed with exception of the water molecule at the distal side of heme.

The energy grid maps of atomic interaction were calculated with a 0.25 Å grid spacing and 120 grid points forming a 30 Å cubic box centered at the active site of peroxidases on the heme side exposed to water. The space of the cubic box covered the active site of peroxidases and the space beyond. The electrostatic interaction energy grid used a distance-dependent dielectric function of *Mehler-Solmajer* [27]. The docking was accomplished using the *Lamarckian* genetic algorithm. The number of individuals in populations was set to 50. The maximum number of energy evaluations of this algorithm is 250000; the maximum number performed was 27000. The number of top individuals guaranteed to survive into the next generation was 1, the crossover and mutation rates were 0.02 and 0.80.

Acknowledgments

The authors express sincere thanks to Dr. *A. J. Olson* for the supply of AutoDock 3.0. We also wish to thank *M. Metzler* and *C. Ludvigsen* for technical assistance.

References

[1] Call HP, Mücke I (1997) J Biotechnol **53**: 163
[2] Dunford HB, Adeniran AJ (1986) Arch Biochem Biophys **251**: 536
[3] Hughes MF, Smith BJ, Eling TE (1992) Chem Res Toxicol **5**: 340
[4] Krikstopaitis K, Kulys J, Pedersen AH, Schneider P (1998) Acta Chem Scand **52**: 469
[5] Kulys J, Krikstopaitis K, Ziemys A (2000) J Biol Inorg Chem **5**: 333
[6] Krikstopaitis K, Kulys J, Palaima A (1996) Biologija **4**: 33
[7] Kulys J, Deussen H-J, Krikstopaitis K, Lolck R, Schneider P, Ziemys A (2000) J Chem Soc Perk T2 (in press)
[8] Schneider P, Deussen H-J (1999) Patent application WO9957360
[9] Marcus RA, Sutin N (1985) Biochim Biophys Acta **811**: 265
[10] Tsukamoto K, Itakura H, Sato K, Fukuyama K, Miura S, Takahashi S, Ikezawa H, Hosoya T (1999) Biochemistry **381**: 2558
[11] Petersen JFW, Kadziola A, Larsen S (1994) FEBS Lett **339**: 291
[12] Baskakov YA, Stonov LD, Bakumenko LA, Mikhno LA, Gorskaya TV, Pokrovskaya NB (1971) Patent GB 71-7819 19710325, CAN 78: 159291
[13] Bamberger E (1919) Chem Ber **52**: 1120
[14] Tisue GT, Grassmann M, Lwowski W (1968) Tetrahedron **24**: 999
[15] Steinbrunn G, Fischer A (1967) BASF-AG Patent FR 1507608; Chem Abstr (1969) EN, 70, 57386e
[16] Baskakow YA, Mel'nikov NN (1958) Khim Nauka I Prom **3**: 683; Chem Abstr (1959) 7062
[17] Oesper RE, Broker W (1925) J Am Chem Soc **47**: 2606
[18] Oxley PW, Adger BM, Sasse MJ, Forth MA (1989) Org Synth **67**: 187
[19] Andersen MB, Hsuanyu Y, Welinder KG, Schneider P, Dunford HB (1991) Acta Chem Scand **45**: 1080
[20] Nelson D, Kiesow LA (1972) Anal Biochem **49**: 474
[21] Frisch MJ, Trucks GW, Schlegel HB, Gill PMW, Johnson BG, Robb MA, Cheeseman JR, Keith T, Petersson GA, Montgomery JA, Raghavachari K, Al-Laham MA, Zakrzewski VG, Ortiz JV, Foresman JB, Cioslowski J, Stefanov BB, Nanayakkara A, Challacombe M, Peng CY, Ayala PY, Chen W, Wong MW, Andres JL, Replogle ES, Gomperts R, Martin RL, Fox DJ, Binkley JS, Defrees DJ, Baker J, Stewart JP, Head-Gordon M, Gonzalez C, Pople JA (1995) Gaussian 94, Revision E. 1, Gaussian, Inc., Pittsburgh PA
[22] Goodsell DS, Olson AJ (1990) Prot Struct Gen **8**: 195
[23] Morris GM, Goodsell DS, Huey R, Olson AJ (1996) J Com Aid Mol Des **10**: 293
[24] Morris GM, Goodsell DS, Halliday RS, Huey R, Hart WE, Belew RK, Olson AJ (1998) J Comp Chem **19**: 1639
[25] Kunishima N, Fukuyama K, Matsubara H, Hatanaka H, Shibano Y, Amachi T (1994) J Mol Biol **235**: 331
[26] Itakura H, Oda Y, Fukuyama K (1997) FEBS Let **412**: 107
[27] Mehler EL, Solmajer T (1991) Protein Eng **4**: 903

Received June 26, 2000. Accepted (revised) August 9, 2000

Verleger: Springer-Verlag KG, Sachsenplatz 4–6, A-1201 Wien. – Herausgeber: Österreichische Akademie der Wissenschaften, Dr.-Ignaz-Seipel-Platz 2, A-1010 Wien, und Gesellschaft Österreichischer Chemiker, Eschenbachgasse 9, A-1010 Wien. – Redaktion: Währinger Straße 38, A-1090 Wien. – Satz und Umbruch: Thomson Press Ltd., New Delhi, India. – Offsetdruck: MANZ CROSSMEDIA, A-1051 Wien. – Verlagsort: Wien. – Herstellungsort: Wien. – Printed in Austria.